

Phase Crossover induced by Dynamical Many Body Localization in Periodically Driven Long-Range Spin Systems

Mahbub Rahaman,¹ Takashi Mori,² and Analabha Roy¹

¹*Department of Physics, The University of Burdwan, Golapbag, Bardhaman - 713 104, India*

²*RIKEN CEMS, 2-1 Hirosawa, Wako, Saitama, 351-0198, Japan*

Dynamical many-body freezing occurs in periodic transverse field-driven integrable quantum spin systems. Under resonance conditions, quantum dynamics causes practically infinite hysteresis in the drive response, maintaining its starting value. We extended this to non-integrable many body systems by reducing the Hamiltonian symmetries through a power-law dependence in spin exchange energy, $J_{ij} = 1/|i - j|^\beta$. The dynamics of the integrable short-range Transverse Field Ising Model (TFIM) and non-integrable long-range Lipkin Meshkov-Glick (LMG) models were investigated. In the LMG, the resonance conditions in the driving field suppresses the heating postulated by the *Eigenstate Thermalization Hypothesis* (ETH) by inducing *Dynamical Many Body Localization*, or DMBL. This is in contrast to Many Body Localization (MBL), which requires disorder to suppress ETH. DMBL has been validated by the Inverse Participation Ratio (IPR) of the quasi-stationary Floquet modes. While TFIM has IPR localization for all drive parameters, the LMG exhibits high-frequency localization only at the resonances. IPR localization in the LMG deteriorates with an inverse system size law at lower frequencies, which indicates heating to infinite temperature. Furthermore, adiabatically increasing frequency and amplitude from low values raises the Floquet state IPR in the LMG from nearly zero to unity, indicating a phase crossover. This occurrence enables a future technique to construct an MBL engine in clean systems that can be cycled by adjusting drive parameters only.

Keywords: Dynamical localization, Thermalization, Phase Crossover

Under certain resonance conditions in the drive parameters, periodically driven quantum many-body systems can experience dynamical many-body freezing (DMF), which causes the response to freeze completely to its initial value at all times [1–3]. This arises as a consequence of additional approximate symmetries that occur at resonance. DMF has been demonstrated via the Rotating Wave Approximation (RWA) in the driven TFIM with nearest-neighbour interactions [4] and is shown to be protected when translational invariance is explicitly broken (say, by disorder) [5, 6].

The utilization of Floquet theory simplifies the analysis of time-periodic systems. For closed quantum systems governed by the time-dependent Schrödinger equation, the *Floquet Hamiltonian* allows for a mapping of the time-dependent dynamics into the dynamics of a time-independent effective Hamiltonian, provided the system is strobed at integer multiples of the time period of the drive. The time independent eigenstates of the effective Hamiltonian correspond to quasi-stationary *Floquet Modes* of the original Hamiltonian. The temporal progression of the system comes from phase coefficients that capture the dynamics [7, 8].

Any sufficiently complex non-integrable Many Body System is expected to thermalize according to the Eigenstate Thermalization Hypothesis (ETH) despite the fact that closed quantum dynamics preserves the memory of the initial state of the system. This arises due to the properties of the matrix elements of observables in typical states[9]. The ETH can be readily adapted to time-periodic systems using Floquet theory (the Floquet-ETH, or FETH). Nonetheless, the conditions for ETH to hold are not particularly strong, and the density matrix of

the system can fail to approach one that is described by a thermal expression. Thermal systems must conduct because they exchange energy and particles internally during thermalization. Thus, insulating systems can be naturally athermal; Many Body Localization (MBL) is a well-studied case [10]. This phenomenon is stable against local perturbations, and constitutes an exotic state of matter with far-reaching implications in theoretical physics, as well as in practical applications[11].

The addition of disorder has been identified as a crucial component in the onset of MBL. In that case, thermalization is prevented by disorder-induced localization. Nonetheless, alternative approaches to MBL in strongly interacting disorder-free systems [12–14], inhomogeneous systems [15–18], and by inducing disorder in the emergent physics [19] and by other effective means [17] (albeit with strong finite-size effects), have been reported. An alternative approach to realizing MBL in disorder-free *homogeneous* many-body systems involve *Floquet Engineering*, where a time-periodic drive is introduced, and the drive parameters tuned to introduce a clustering of quasistationary energies in a manner similar to localization[9].

In this article, we use the fact that emergent approximate symmetries can be engineered in Floquet systems and apply it to long-range interactions. This results in *Dynamical Many Body Localization* (DMBL) at resonant values of the drive parameters, and complete thermal behaviour at other values. This phenomenon is distinct from DMF in the TFIM, since clean TFIM systems, being integrable, never thermalize.

To demonstrate the onset of MBL, we investigate the driven Lipkin-Meshkov-Glick (LMG) model[20–25],

⁷³ a long-range system that extends the nearest-neighbour
⁷⁴ interactions in the TFIM to all-to-all interactions. [26–28]
⁷⁵ We have recovered the onset of DMF in this system and
⁷⁶ have supported our result with numerical simulations.

⁷⁷ In addition, we compare the degree of localization of
⁷⁸ the quasi-stationary Floquet modes in the LMG model
⁷⁹ with the TFIM. In order to do so, we look at the Inverse
⁸⁰ Participation Ratio (IPR) of the Floquet modes in the
⁸¹ representation given by the eigenstates of the symmetry-
⁸² breaking field. The IPR, closely related to the concept
⁸³ of quantum purity, is defined as the formal sum of the
⁸⁴ square of the density in some physically meaningful space
⁸⁵ or representation. A high IPR of a stationary state de-
⁸⁶ notes low participation in most of the representation, and
⁸⁷ a low IPR distributes participation uniformly across the
⁸⁸ representation, leading to ergodic dynamics[29]. Thus,
⁸⁹ IPR [30] is a useful tool for witnessing MBL of a quan-
⁹⁰ tum system. For an MBL system, the IPR is unity, and
⁹¹ it scales inversely with the number of spins when it is
⁹² thermally distributed [31].

⁹³ In the first section of this paper, we present all es-
⁹⁴ sential theoretical frameworks. Our results for the LMG
⁹⁵ model are presented next in section II. In that section,
⁹⁶ we have used the Rotating Wave Approximation (RWA)
⁹⁷ [32], where only the slowest rotating terms in the Fourier
⁹⁸ expansion of the Hamiltonian in a frame co-rotating with
⁹⁹ the symmetry breaking drive field are retained. In addi-
¹⁰⁰ tion, we have the obtained numerical simulations of the
¹⁰¹ Floquet modes and their IPR. They are used to probe
¹⁰² the system dynamics in the high and low-frequency do-
¹⁰³ mains at both limits of β . In section III we have used
¹⁰⁴ phase space plots to contrast the low and high frequency
¹⁰⁵ limits of the LMG model in the thermodynamic limit by
¹⁰⁶ mapping it to an equivalent classical Hamiltonian sys-
¹⁰⁷ tem. Finally, in section IV, we have looked at numerical
¹⁰⁸ computations of the IPR of the Floquet modes for dif-
¹⁰⁹ ferent values of the drive parameters, well beyond those
¹¹⁰ that allow for the RWA. We observed that, if the system
¹¹¹ is driven by an adiabatically increasing drive frequency
¹¹² from low to high limit while remaining in the resonance
¹¹³ region, a sharp crossover from a thermal to an MBL phase
¹¹⁴ occurs. We conclude with discussions and outlook.

¹¹⁵

I. BACKGROUND

¹¹⁶ The Eigenstate Thermalization Hypothesis (ETH) is a
¹¹⁷ series of conjectures that allows for the thermalization of
¹¹⁸ an isolated quantum many body system. The state of
¹¹⁹ the system, $|\psi(t)\rangle$, evolves according to the Schrödinger
¹²⁰ equation $\hat{H}|\psi(t)\rangle = i\frac{\partial}{\partial t}|\psi\rangle$. The Hamiltonian \hat{H} is as-
¹²¹ sumed to be *non-integrable*, in that it lacks an extensive
¹²² number of conserved quantities that can be written as a
¹²³ sum of local operators, that is to say, there are no set of
¹²⁴ observables $\hat{O}_s = \sum_i \hat{L}_i$ such that $[\hat{O}_s, \hat{H}] = 0$. Here,
¹²⁵ the \hat{O}_s constitute an arbitrary CSCO (complete set of

¹²⁶ commuting observables), and \hat{L}_i are *local*, each having
¹²⁷ sub-extensive support in the system [33]. In addition, we
¹²⁸ postulate an "equilibrium" value A_{eq} for every observable
¹²⁹ \hat{A} , such that

$$A_{eq}(E) \equiv \frac{\text{Tr}(\hat{A}e^{-\beta\hat{H}})}{\text{Tr}(e^{-\beta\hat{H}})}, \quad (1)$$

¹³⁰ where $E = \langle\psi(t)|\hat{H}|\psi(t)\rangle$ is the conserved energy of the
¹³¹ system, and $\beta = 1/(k_B T)$ is the inverse temperature, H_{eq}
¹³² is an effective Hamiltonian that captures the long-time
¹³³ average dynamics of the system, and k_B is the Boltzmann
¹³⁴ constant.

To put it simply, ETH proposes that this many-body Hamiltonian undergoes thermalization as seen in the *long-time averages* of observables, with the eigenstates bearing resemblance to thermal states. The aforementioned hypothesis serves as a valuable instrument for comprehending the conduct of stimulated quantum systems and their correlation with thermal equilibrium. This assertion can be justified by examining the expectation value of an observable \hat{A} as it evolves under the Schrödinger equation. To see this, we first expand the state of the system $|\psi(t)\rangle$ as:

$$|\psi(t)\rangle = \sum_m c_m(t) |m(0)\rangle,$$

¹³⁵ where $|m(0)\rangle$ represents the eigenstates of $\hat{H}(0)$ with
¹³⁶ energy E_m . The coefficients $c_m(t)$ describe the time-
¹³⁷ dependent amplitude of the expansion. Plugging these
¹³⁸ expansions into the expression for the expectation value,
¹³⁹ we obtain the long-time average of the expectation
¹⁴⁰ value [34]:

$$\overline{\langle \hat{A}(t) \rangle} = \sum_{m,k} \overline{c_m^*(t)c_k(t)} \langle m(0)|\hat{A}|k(0)\rangle, \quad (2)$$

¹⁴¹ where the overline indicates the following operation for
¹⁴² any time-dependent quantity $\mathcal{O}(t)$,

$$\overline{\mathcal{O}} \equiv \lim_{t \rightarrow \infty} \frac{1}{t} \int_0^t d\tau \mathcal{O}(\tau). \quad (3)$$

The matrix elements $\langle m(0)|\hat{A}|k(0)\rangle$ are said to satisfy the Srednicki ansatz [35, 36]:

$$\begin{aligned} \langle m(0)|\hat{A}|k(0)\rangle &\approx A_{eq} \left(\frac{E_m + E_k}{2} \right) \delta_{mk} + \\ &e^{-\frac{1}{2}S\left(\frac{E_m+E_k}{2}\right)} f\left(\frac{E_m + E_k}{2}, E_m - E_k\right) R_{mk}. \end{aligned} \quad (4)$$

Here, S is the thermodynamic entropy and R_{mk} are elements of a random matrix with vanishing mean and unit variance. What this means for the ensuing dynamics is that the system explores the accessible Hilbert space uniformly, and the matrix elements $\langle m(0)|\hat{A}(t)|k(0)\rangle$ become indistinguishable for most pairs of m and k . Applying this ansatz and taking the thermodynamic limit

by ignoring terms $\mathcal{O}(e^{-S/2})$, the expression for the expectation value becomes:

$$\begin{aligned}\langle \hat{A}(t) \rangle &\approx \sum_m \overline{|c_m(t)|^2} A_{eq}(E_m) \\ &\approx A_{eq}(E) \sum_m \overline{|c_m(t)|^2} = A_{eq}(E),\end{aligned}$$

where, in the last step, we utilized the fact that A_{eq} is a smooth function, and that the states with energies far from E have $|c_m(t)|^2 \approx 0$. Therefore, in the limit of large systems the expectation value of an observable \hat{A} is approximately equal to the thermal expectation value A_{eq} . This is the essence of the ETH, which suggests that individual eigenstates of a quantum system can be described by statistical mechanics in the long-time limit.

We now generalize the ETH to non-integrable many body systems that are closed, but not isolated. In that case, it is possible to impart a periodic time-dependence on the Hamiltonian while still ensuring unitary evolution. If the time period of the drive is T , and the corresponding drive frequency $\omega \equiv 2\pi/T$, the Floquet theorem states that the solutions to the Schrödinger equation can be written as $|\psi(t)\rangle = e^{-i\epsilon t/\hbar} |\phi(t)\rangle$, where the $|\phi(t)\rangle$ are T -periodic states called *Floquet Modes*, the corresponding $\epsilon \in \mathbb{R}$, are called *quasienergies*. Quasienergy values are not unique, and can be made to be bounded within a Floquet Brillouin zone, *viz.* a range $[-\omega/2, \omega/2]$ [37, 38]. As a consequence, the unitary evolution operator can be split into two parts as follows [39].

$$U(t) = e^{-i\hat{K}_F(t)} e^{-i\hat{H}_F t}. \quad (5)$$

Here, the micromotion operator $\hat{K}_F(t)$ is time-periodic in T , with $\hat{K}_F(0) = 0$, and the Floquet Hamiltonian $\hat{H}_F = e^{i\hat{K}_F(t)} [\hat{H}(t) - i\partial_t] e^{-i\hat{K}_F(t)}$. Thus, if the system is strobed at integer multiples of T only, then the unitary evolution matches that of a time independent Hamiltonian H_F . This can capture most of the exact dynamics at large frequencies. In such systems, the *Floquet Eigenstate Thermalization Hypothesis* (FETH) posits that, subject to specific conditions and in the context of a system of significant size, the Floquet modes themselves exhibit thermal state-like behavior, *i.e.*, $\hat{H} \approx \hat{H}_F$ in eqn 1. However, in contrast to the isolated systems, the loss of energy conservation allows for the mixing of all Floquet modes in the ensuing dynamics, not just those with quasienergies near E . Were this to actually happen in the ensuing dynamics, it can be reconciled with ETH by ensuring that the RHS of eqn 1 is independent of β , *i.e.*, an infinite temperature ensemble [40]. In other words, the nonequilibrium steady state of the system tends to an infinite temperature, maximum entropy density matrix.

However, drive parameters like amplitude, frequency, and duty-cycle strongly affect the structure of the Floquet modes $|\phi\rangle$. Thus, they can be engineered to prevent the kind of full mixing that would lead to infinite tem-

peratures, manifesting suppression of thermalization dynamically. Thus, this type of *Floquet Engineering* can produce *Dynamical Many Body Localization* (DMBL), where the system fails to reach thermal equilibrium and remains localized, possibly near its initial state, even at large times. This paradigm seems similar to standard Many-Body Localization[41, 42], where disorder, locality, and integrability can cause athermality via breakdown in the Srednicki ansatz. However, DMBL stems from periodic driving, and thus can occur regardless of disorder, locality of observables, or system integrability, all of which have been studied for MBL onset [43–45].

Integrable Many Body systems do not exhibit thermalization. When subjected to time-periodic drives, Floquet engineering allows for the introduction of additional approximate conserved quantities that dynamically suppress the evolution of certain observables by hysteresis. This type of *freezing* of response has been shown in integrable systems [6]. A paradigmatic example is the driven Transverse Field Ising model (TFIM) in one dimension [46]. The Hamiltonian is given by

$$\hat{H}(t) = \hat{H}_0 + h_z(t) \hat{H}_1, \quad (6)$$

$$\hat{H}_0 = -\frac{1}{2} \sum_{i=1}^N \sigma_i^x \sigma_{i+1}^x, \quad (7)$$

$$\hat{H}_1 = -\frac{1}{2} \sum_{i=1}^N \sigma_i^z. \quad (8)$$

Here, the undriven Hamiltonian \hat{H}_0 consists of nearest-neighbour interactions between N number of spin-1/2 particles on a one-dimensional spin network. The transverse field is denoted by \hat{H}_1 , and is being varied by a time-periodic and harmonic signal $h_z(t) = h_0 + h \cos \omega t$, yielding a time period $T = 2\pi/\omega$ with amplitude h , drive frequency ω , and d.c. field h_0 . This Hamiltonian can be readily transformed into a spinless pseudo-fermionic system via the Jordan-Wigner transformation [4]. When written in momentum space spanned by spinors $\psi_k = (c_{-k}, c_k^\dagger)^T$ of fermions at momentum k created (annihilated) by operators c_k^\dagger (c_k), the effective Hamiltonian

$$H(t) = \sum_{(k, -k)-\text{pairs}} \psi_k^\dagger \left[\left(f_k - h_z(t) \right) \tau_z + \tau_x \Delta_k \right] \psi_k, \quad (9)$$

where $f_k = \cos k$, $\Delta_k = \sin k$, τ_{xyz} are the three Pauli Matrices, and the sum is over distinct $(k, -k)$ Cooper Pairs. We can transform our system to a frame that rotates with the time-varying symmetry-breaking field. This is achieved by the means of the unitary transformation operator

$$U(t) = \prod_k U_k(t) \quad (10)$$

$$U_k(t) = \exp \left\{ \left[\frac{i\hbar}{\omega} \sin \omega t \right] \tau_z \right\}.$$

The resulting transformed Hamiltonian $H'(t) = U^\dagger(t) H(t) U(t) - iU^\dagger(t) \partial_t U(t)$ simplifies to

$$H'(t) = \sum_{(k,-k)-\text{pairs}} \psi_k^\dagger \left[\tau_z f_k + \tau_x \cos(\eta \sin \omega t) + \tau_y \sin(\eta \sin \omega t) \right] \psi_k, \quad (11)$$

where we defined $\eta = 2h/\omega$. Using the Jacobi-Anger formula [47]

$$e^{i\eta \sin \omega t} = \sum_{n=-\infty}^{\infty} J_n(\eta) e^{in\omega t}, \quad (12)$$

where $J_n(\eta)$ are Bessel Functions, the transformed Hamiltonian simplifies to

$$H'(t) = \sum_{(k,-k)} \psi_k^\dagger \left\{ \tau_z f_k + 2\tau_x \Delta_k \sum_{n \geq 0} J_{2n}(\eta) \cos(2n\omega t) - 2\tau^y \Delta_k \sum_{n \geq 0} J_{2n+1}(\eta) \sin[(2n+1)\omega t] \right\} \psi_k. \quad (13)$$

In the frequency regime $\omega \gg f_k$, the long-time average $H^{RWA} \equiv \lim_{n \rightarrow \infty} \frac{1}{nT} \int_0^{nT} dt H'(t)$ can serve as a suitable approximation for $H'(t)$. This approximation, known as the *Rotated Wave Approximation* (RWA), eliminates the oscillating modes and results in an effective Hamiltonian that is independent of time,

$$H^{RWA} = \sum_{(k,-k)-\text{pairs}} \psi_k^\dagger \left[f_k \tau_z + 2J_0(\eta) \Delta_k \tau_x \right] \psi_k. \quad (14)$$

It is evident that by manipulating the drive parameters, specifically the amplitude denoted by h and the frequency denoted by ω , in a manner such that η is positioned on a root of $J_0(\eta)$, the fermion number can be conserved to a significant extent at this particular resonance. Consequently, it is feasible to exercise direct control over H^{RWA} , resulting in a comprehensive suppression of the dynamics of otherwise responsive observables.

This phenomenon is highly general in nature, and can be readily adapted to non-integrable systems. In such cases, freezing has the additional effect of inducing DMBL, suppressing thermalization to infinite temperatures. Numerical quantification of localization of a specific (quasi) stationary state in a physically significant representation can be achieved through the computation of the *Inverse Participation Ratio* (IPR). The IPR is generally defined as the formal sum over the square of the local density in a physically meaningful space. [48–51] In the single particle case, the IPR, for a state $|\psi\rangle$ can be written as

$$\phi_{IPR} \equiv \int dx |\langle x | \psi \rangle|^4.$$

This definition can be applied to obtain the IPR of a state $|\phi\rangle$ in a representation given by any single particle basis $|m\rangle$ as

$$\phi_{IPR} \equiv \sum_m |\langle m | \psi \rangle|^4. \quad (15)$$

The smallest value of the IPR corresponds to a fully delocalized state, $\psi(x) = 1/\sqrt{N}$ for a system of size N [51, 52]. Values of the IPR close to unity correspond to localized states [53]. For a periodically driven system, we look at the IPR of the quasi-stationary Floquet modes at $t = T$, where $t = 2\pi/\omega$ for drive frequency ω . In the TFIM model, equation 14 indicates that, at resonance, when $J_0(\eta) = 0$, the Floquet modes are approximately given by the fermionic Fock states, which have a trivially unit IPR in the representation of the eigenmodes of the transverse field \hat{H}_1 in equation 6. Here, a particular Floquet mode can be decomposed into a direct product of cooper-pair states as $|\phi\rangle = \prod_{k,-k} |\phi_k^n\rangle$. In the RWA limit and at resonance, $|\phi_k^n\rangle$ has values of $|0\rangle, |k, -k\rangle$ for two values of $n = 0, 1$ respectively. We define the reduced IPR of $|\phi_k^n\rangle \forall k$ to be

$$\phi_{IPR}^{(n)}(k) = |\langle 0 | \phi_k^n \rangle|^4 + |\langle +k, -k | \phi_k^n \rangle|^4, \quad (16)$$

where $n = 0, 1$. The full many-body IPR can be obtained from the reduced IPR in eqn 16 by a product over all momenta in the Brillouin zone, yielding

$$\phi_{IPR} = \prod_k \phi_{IPR}^{(n)}(k). \quad (17)$$

In the RWA limit and at resonance, this quantity is unity, indicating very low participation and the onset of freezing. Figure 1 shows results from numerically simulating the TFIM dynamics. The reduced IPR for a particular Floquet mode recovered by simulating the exact Schrödinger dynamics over a single time period of the drive, and plotted as a function of momentum k for different η 's. At resonance, when η lies at the root of the Bessel function $J_0(\eta)$, the Reduced IPR is nearly unity for all momenta. Consequently, so is ϕ_{IPR} . Outside this resonance, the IPR is unity only for some momenta because the effective Hamiltonian is perfectly diagonal at

$k \in \{-\pi, 0, \pi\}$ as can be seen in the cross-sectional plots of figure 1. As we move away from the resonance point, the full IPR decreases exponentially as a power law in the system size, as can be seen in the bottom-right panel of fig 2. However, as the TFIM is an integrable spin model, the IPR never drops to a value that is small enough to indicate thermalization. This can be seen in the bottom panels of figure 2, where the power-law decay of $\phi_{IPR}(N)$ never approaches the thermodynamic scaling law $\phi_{IPR}(N) \sim 2^{-N}$ for either small or large frequencies. Note that, at low frequencies, RWA complete localization fails due to the unavailability of zero off-diagonal terms in the effective transformed Hamiltonian, as well as the absence of integrability breaking terms to counteract the

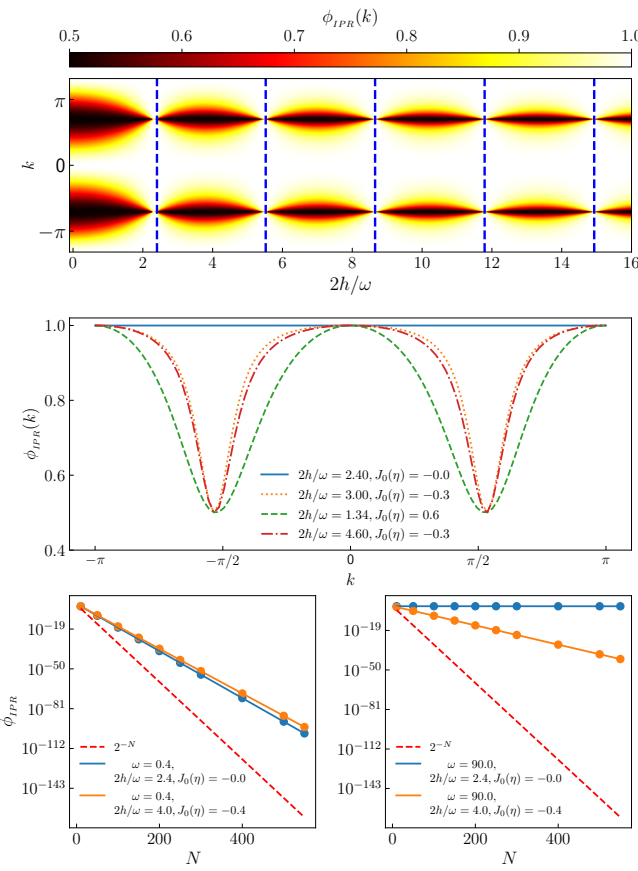


FIG. 1. Reduced IPR (defined in equation 16) for one of the two Floquet modes obtained from the exact dynamics of the TFIM for size $N = 100$ and $\omega = 90$ for the entire Brillouin zone (top panel, ordinate) and a few drive amplitudes (top panel, abscissa). The dashed lines (top panel) indicate the roots of $J_0(\eta)$. The middle panel shows cross-sections of the reduced IPR in k -space for four chosen amplitudes. Finally, the bottom panels show semi-log plots of the scaling with N of the full many body IPR as defined in eqn 17, with the left panel for a small $\omega = 0.4$, amplitude h chosen to lie both in and out of the root of $J_0(\eta)$ as indicated in the legend, with similar plots on the right panel for a large $\omega = 90$.

off diagonal terms. Because the TFIM can be mapped to a system of noninteracting particles as shown in eqn 9, it is not physically meaningful to refer to the unit IPR region as "*Many Body Localization*", because the parameter space lacks a thermalized region to contrast with this state. The type of Floquet Engineering described above, on the other hand, can be easily applied to a broad class of nonintegrable systems where FETH is expected to hold in certain regions. Long-range spin systems, in particular, where the exchange energies between far-off spins are taken into account in the model Hamiltonian, are good candidates because they are known to thermalize when driven with low frequencies [54].

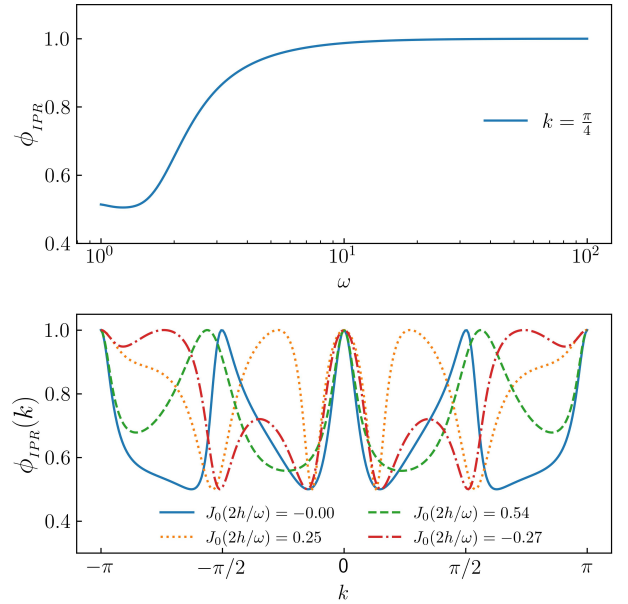


FIG. 2. Reduced IPR obtained by adiabatically increasing ω (top panel abscissa) for one the floquet mode obtained from equation 16 at the root of $J_0(\eta)$ for $N = 500$. IPR is ~ 0.5 (localized yet not fully freezing) upto $\omega \sim 2$, after that, smoothly increased to unity (fully localized and freezing) at higher $\omega \geq 10$ (top panel, ordinate). At bottom panel cross-sections for four chosen amplitudes at $\omega = 2$ are plotted for a brillouin zone (abscissa) with corresponding reduced IPRs (ordinate).

II. LONG RANGE INTERACTIONS: THE LIPKIN MESHKOV GLICK MODEL:

The periodically driven Lipkin Meshkov Glick (LMG) model [20, 55] for N long-range spins is described by the Hamiltonian

$$\hat{H}(t) = \hat{H}_0 + [h \cos(\omega t) + h_0] \hat{H}_1. \quad (18)$$

Here, the undriven part \hat{H}_0 and the driven part \hat{H}_1 are, respectively,

$$\begin{aligned} \hat{H}_0 &= \frac{2}{N-1} \sum_{ij} \hat{\sigma}_i^z \hat{\sigma}_j^z, \\ \hat{H}_1 &= \sum_{i=1}^N \hat{\sigma}_i^x. \end{aligned} \quad (19)$$

The Kac-norm of $2/(N-1)$ arises from the choice to maintain the extensivity of the interaction energy. The Hamiltonian in equation 18 commutes with $P_{ij} \equiv \frac{1}{2}(1 + \vec{\sigma}_i \cdot \vec{\sigma}_j)$. In addition, it also commutes with the total angular momentum $S^2 = |\vec{S}|^2$, where $\vec{S} = S^x \hat{x} + S^y \hat{y} + S^z \hat{z} \equiv \frac{1}{2} \sum_i \vec{\sigma}_i$. We now choose to populate the sys-

tem in a state with $S^2 = \frac{N}{2} \left(\frac{N}{2} + 1 \right)$. In that case, the dynamics remains invariant in the $N + 1$ -dimensional space spanned by the common eigenstates of $P_{ij}, |S|^2$ and S_z ; the so-called *Totally Symmetric Subspace*, or TSS [56]. Let the eigenvalues of S^z in the TSS be s_n , and the eigenvectors be $|s_n\rangle$. Here, $s_n = -\frac{1}{2} + \frac{n}{N}$ and the index $n = 0(1)N$ has $N + 1$ values. The dynamics is restricted to this invariant subspace, wherein the matrix elements of the Hamiltonian are given by

$$\begin{aligned}\langle s_i | \hat{H}_0 | s_j \rangle &= -\frac{4}{N-1} s_i^2 \delta_{ij}, \\ \langle s_i | \hat{H}_1 | s_j \rangle &= \left[\sqrt{\frac{N}{2} \left(\frac{N}{2} + 1 \right) - N s_i (N s_{i+1})} \delta_{i+1,j} \right. \\ &\quad \left. + \sqrt{\frac{N}{2} \left(\frac{N}{2} + 1 \right) - N s_i (N s_{i-1})} \delta_{i-1,j} \right].\end{aligned}\quad (20)$$

These allow for a numerical representation of the Hamiltonian in the TSS.

³⁰¹ Next, we transform the Hamiltonian to the rotated frame given by the operator

$$\hat{U}(t) = \exp \left[i \frac{h}{\omega} \sin(\omega t) \hat{H}_1 \right]. \quad (21)$$

³⁰³ This is analogous to the rotation performed for the TFIM ³⁰⁴ in eqns 10 and 11. Defining $\tau = \frac{h}{\omega} \sin \omega t$, we use the fact ³⁰⁵ that $\hat{H}_1 = 2S^x$, as well as the following identity obtained ³⁰⁶ by using the Baker-Campbell-Hausdorff formula,

$$e^{i2\tau \hat{S}^x} \hat{S}^z e^{-i2\tau \hat{S}^x} = \hat{S}^z \cos(2\tau) + \hat{S}^y \sin(2\tau), \quad (22)$$

to simplify the transformed Hamiltonian $\tilde{H}(t) = \hat{U}^\dagger(t) \hat{H}(t) \hat{U}(t) - \hat{U}^\dagger(t) \partial_t \hat{U}(t)$, yielding

$$\begin{aligned}\tilde{H}(t) &= -\frac{1}{N-1} \left[(S^z)^2 (1 + \cos 4\tau) + (S^y)^2 (1 - \cos 4\tau) \right. \\ &\quad \left. + \{S^y, S^z\} \sin 4\tau \right] - 2h_0 S^x.\end{aligned}\quad (23)$$

²⁹⁹ These allow for a numerical representation of the Hamil- ³⁰⁷ Next, we define $\eta \equiv 4h/\omega$ and use the Jacobi-Anger for- ³⁰⁸ mula in eqn 12 to expand $\tilde{H}(t)$. This yields

$$\begin{aligned}\tilde{H}(t) &= -\frac{\hat{S}^2}{N-1} + \frac{(\hat{S}^x)^2}{N-1} - 2h_0 \hat{S}^x - \frac{J_0(\eta)}{N-1} \left[(\hat{S}^z)^2 - (\hat{S}^y)^2 \right] - \frac{2}{N-1} \left[(\hat{S}^z)^2 - (\hat{S}^y)^2 \right] \sum_{k=1}^{\infty} J_{2k}(\eta) \cos(2k\omega t) \\ &\quad - \frac{2}{N-1} \{ \hat{S}^y, \hat{S}^z \} \sum_{k=1}^{\infty} J_{2k-1}(\eta) \sin[(2k-1)\omega t].\end{aligned}\quad (24)$$

If ω is large enough to smooth out the harmonic components, we obtain the RWA,

$$\begin{aligned}\tilde{H}(t) \approx \tilde{H}_{\text{RWA}} &\equiv -\frac{\hat{S}^2}{N-1} + \frac{(\hat{S}^x)^2}{N-1} - 2h_0 \hat{S}^x \\ &\quad - \frac{J_0(\eta)}{N-1} \left[(\hat{S}^z)^2 - (\hat{S}^y)^2 \right].\end{aligned}\quad (25)$$

³⁰⁰ If the drive amplitude h is adjusted such that η lies at ³¹¹ a root of $J_0(\eta)$ (the localization point), the RWA Hamil- ³¹² tonian is diagonal in the representation of the simultane- ³¹³ ous eigenstates of transverse field \hat{S}^x , and S^2 , yielding an ³¹⁴ IPR of unity in that representation, similar to the TFIM ³¹⁵ in the previous section. Note however, that if the DC ³¹⁶ transverse field h_0 is set to 0, then, at the localization ³¹⁷ point, the RWA Hamiltonian $\tilde{H}_{\text{RWA}} \sim (\hat{S}^x)^2$ in the TSS. ³¹⁸ The eigenvalues are two-fold degenerate. This produces ³¹⁹ infinitely many (Floquet) eigenmodes in the degenerate ³²⁰ subspace whose IPRs may not always be unity in the S^x ³²¹ representation. The removal of this degeneracy necessi- ³²² tates the inclusion of the d.c. field h_0 . However, note ³²³ that rational values of h_0 may add accidental degenera-

³²⁴ cies in \tilde{H}_{RWA} . To see this, note that, at a localization ³²⁵ point, the eigenvalues of \tilde{H}_{RWA} in the TSS are given by

$$\text{Eigs} \left[\tilde{H}_{\text{RWA}} \right] = \frac{\left(\frac{N}{2} - m \right)^2}{N-1} - 2h_0 \left(\frac{N}{2} - m \right), \quad (26)$$

³²⁶ where the half-integer $-N/2 \leq m \leq N/2$ is the eigen- ³²⁷ value corresponding to a particular eigenstate $|m\rangle$ of the ³²⁸ symmetry-breaking field \hat{S}^x . In order to ensure that no ³²⁹ additional degeneracies occur, we have to set h_0 in such a ³³⁰ way that no two energies accidentally coincide. If $N \gg 1$ ³³¹ (substantially large), then this condition can be readily ³³² met by assuring that $(1 - 2h_0)^{-1}$ is never an integer that ³³³ is divisible by N . To ensure this in our numerical simu- ³³⁴ lations, we have kept h_0 at a small irrational value. The ³³⁵ localization of the Floquet states at resonance is sup- ³³⁶ ported by exact numerical results, as can be seen in the ³³⁷ phase diagram fig 3. Here, we have plotted the arith- ³³⁸ metic mean over all Floquet states of the IPR in the TSS ³³⁹ for each point in the $h - \omega$ plane for $N = 100$ spins. The ³⁴⁰ IPR in S^x representation is

$$\phi_{\text{IPR}}(n) = \sum_m |\langle m | \phi^n \rangle|^4. \quad (27)$$

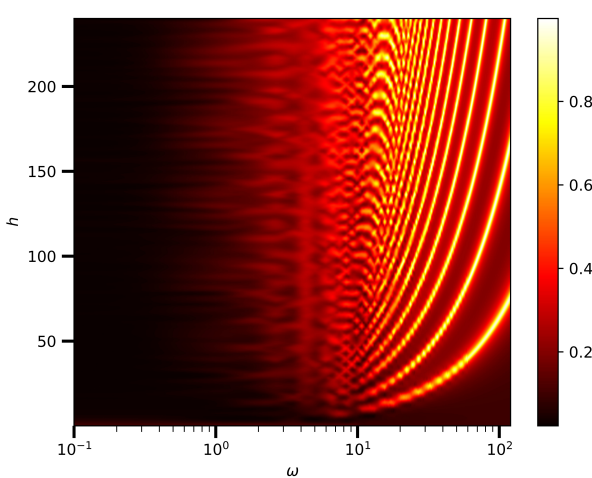


FIG. 3. Plot of the numerically averaged IPR (IPR computed using eqn 27) in the TSS plotted in the $h-\omega$ plane for $N = 100$ spins. In order to display the thermalized region more clearly, ω is plotted on a logarithmic scale on the abscissa. Note that, since the IPR is clearly non-negative, an average IPR of zero means that all Floquet states have zero IPR. Furthermore, the boundedness of IPR in $\phi_{IPR}(n) \leq 1$ ensures that if the average IPR is unity, then all Floquet states have unit IPR.

As can be readily seen in the figure, the IPR is essentially zero when $\omega \lesssim 1$. There is considerable structure in the phase diagram for larger drive frequencies, and along the lines given by the roots of $J_0(\eta)$, the IPR is essentially unity, in agreement with eqn. 25.

In figure 4, we show plots of the IPR of the Floquet modes $|\phi^n\rangle$ for $S^2 = (N/2)(N/2 + 1)$. These plots were obtained numerically by diagonalizing the propagator $U(t)$ at $t = T$, where $U(t)$ is defined in eqn 5. This propagator was obtained from simulations of the exact quantum dynamics using QuTiP, the Quantum Toolbox in Python [57]. We kept the frequency at a fairly large value $\omega = 90$ where we expect that RWA would be valid, and $N = \mathcal{O}(10^2)$. The density plot in the upper panel of fig 4 depicts the IPR of the Floquet states; the abscissa $\eta = 4h/\omega$ and the ordinate is $n/(2N + 1)$, where $n \leq 2N$ is a non-negative integer that indexes the Floquet states in increasing order of m . The dashed vertical lines correspond to the roots of $J_0(\eta)$. Comparing with the IPR of the TFIM in fig 1, we can see a very similar patterns in the immediate neighbourhood of the roots. Evidently, the IPR approaches a value of one for sufficiently large values of the roots, strongly suggesting full DMBL. Deviations occur at the smallest root of $J_0(\eta)$ (around $\eta = 2.405$) due to the contributions from higher order terms in eq 24. Thus, a higher root is favored for DMBL.

The bottom panel of fig 4 contains cross sections of the full IPR plot for selected values of η as indicated in the legend. When the drive amplitude h is adjusted such that η is close to a root of $J_0(\eta)$, the Floquet States are

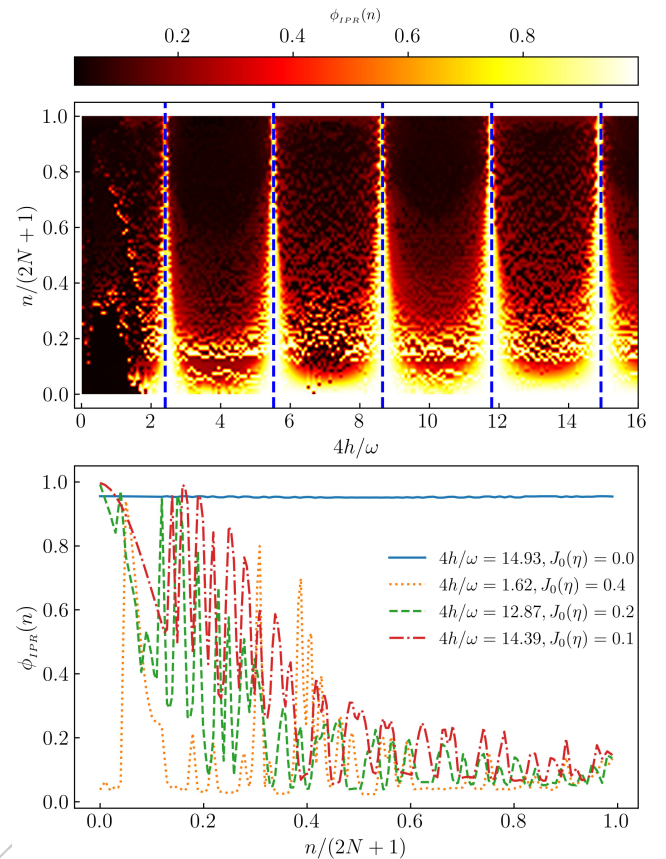


FIG. 4. IPR density plot for all possible Floquet modes (top panel ordinate) for different values of $\eta = 4h/\omega$ (top panel abscissa), deduced from equation 27 for exact LMG Hamiltonian for $N = 50$. Blue dashed lines are roots of $J_0(\eta)$. At bottom panel cross-section of IPR (ordinate) for four different η 's plotted for all possible floquet modes(bottom panel, abscissa) at $\omega = 90$. IPR founds to be \sim unity for all Floquet modes at roots of J_0 .

mixed, but not entirely thermal, since the IPR does not fall to $\mathcal{O}(N^{-1})$, indicating that localization persists to some extent. However, the further we are from the roots, the closer the IPR gets to one predicted by thermalization.

Figure 5 shows plots of the long-time average (from $t = 0 - 200T$) of the field amplitude $\langle \hat{S}^x \rangle$ as a function of η . The system is started from the fully polarized state $s_n = N/2$ in the TSS and the dynamics simulated. The average is plotted for different values of amplitude h , keeping the frequency fixed at a high value of $\omega = 90$. It is clearly very close to unity at roots of $J_0(\eta)$ and falls at points away from it, indicating that S^x is approximately conserved at the localization points.

Small deviations do occur due to the role of higher order terms in the rotated Hamiltonian in eq 23. This can be demonstrated quantitatively by comparing the IPR obtained from the exact dynamics simulation with that obtained from the dynamics of $\tilde{H}(t)$ in eq. 23 af-

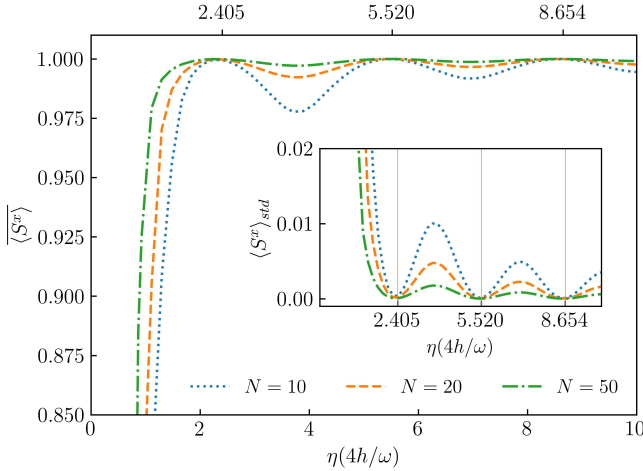


FIG. 5. Temporal average of $\langle \hat{S}^x \rangle$ (ordinate) for different η 's (abscissa) is plotted for $\sim 200T$ at higher ω for different $N=10, 20, 50$. $\langle \hat{S}^x \rangle$ is found to be unity at roots of $J_0(\eta)$. At points away from resonance points, $\langle \hat{S}^x \rangle$ falls below unity. The corresponding standard deviation $\langle \hat{S}^x \rangle_{\text{std}}$ supports the variation of $\langle \hat{S}^x \rangle$ (inset fig.). $\langle \hat{S}^x \rangle_{\text{std}}$ is ~ 0 describing a full freezing of the system at roots of $J_0(\eta)$ (red vertical solid lines).

392 ter truncating the series at orders $k \geq 1$. This com-
 393 parison can be seen in fig 6. The IPR plots from the
 394 exact dynamics indicate that the first localization point,
 395 represented by the lowest root of $J_0(\eta)$, does not show
 396 complete DMBL. However, DMBL is particularly con-
 397 spicuous at large roots. The IPRs of the Floquet states
 398 obtained from the RWA dynamics exhibit large devia-
 399 tions from unity when away from the localization point
 400 as evidenced by the green and red curves in the middle
 401 panel of fig 6. However, complete localization is seen in
 402 the RWA dynamics at any localization point, in contrast
 403 to the exact case in the top panel. Thus, it is necessary
 404 to incorporate higher-order corrections into the Rotating
 405 Wave Approximation (RWA) at lower localization points.
 406 The application of the first-order correction to RWA in
 407 the lower panel of fig 6 results in a curve structure that
 408 is closer to that from the exact dynamics.

III. PERSISTENCE OF DMBL IN THE CONTINUUM LIMIT

410 In the continuum limit, where $N \rightarrow \infty$, the dis-
 411 parity between neighboring values of s_i in equation 20 can
 412 be disregarded, and s_i can be mapped to a continuum
 413 $q \in [-1/2, 1/2]$ [56]. We define the Hamiltonian per par-
 414 ticle $h(t) \equiv \frac{H(t)}{N}$, and a canonically conjugate co-ordinate
 415 $Np \equiv \langle -i \frac{\partial}{\partial q} \rangle$. Then, in this limit, the dynamics can be

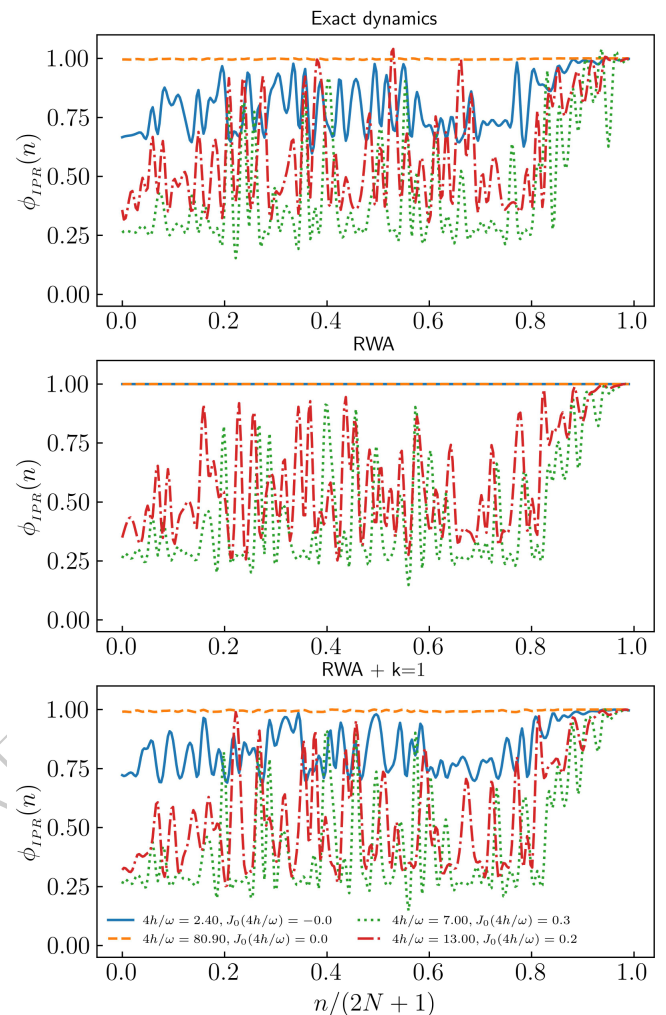


FIG. 6. The comparison between IPR for exact dynamics and RWA with corresponding correction orders. IPR is calculated for four different η 's and corresponding $J_0(\eta)$ values for colors, Blue : $\eta = 2.40, J_0(\eta) = 0.0$, dashed orange: $\eta = 80.9, J_0(\eta) = 0.0$, Green: $\eta = 7.0, J_0(\eta) = 0.3$, Red: $\eta = 13, J_0(\eta) = 0.2$. At low root of $J_0(\eta)$ IPR is not unity (Blue curve) where at higher root (orange dashed) it is unity while at points away from roots IPR are less than unity in the exact (top panel) plot. RWA does not matches with the exact plot. At all roots of $J_0(\eta)$ IPR is unity(middle panel). RWA with additional higher order terms exhibit similar system pattern(Bottom panel) with exact dynamics.

418 approximated by that of a classical Hamiltonian [58]

$$h(t) = -2q^2 - [h \cos \omega t + h_0] \sqrt{1 - 4q^2} \cos p, \quad (28)$$

which yields the dynamical system

$$\begin{aligned}\frac{dq}{dt} &= \frac{\partial h}{\partial p} = h(t)\sqrt{1-4q^2}\sin p \\ \frac{dp}{dt} &= -\frac{\partial h}{\partial q} = 4q\left[1 - \frac{h(t)\cos p}{\sqrt{1-4q^2}}\right],\end{aligned}\quad (29)$$

where $h(t) = [h \cos \omega t + h_0]$. We have profiled simulations of the ensuing dynamics with the *Poincaré surface of section* (PSOS) of the full dynamics. Here, the (q, p) -phase space is strobed at $t = nT$, and plotted for a large number of initial conditions. The results are shown in the upper panels of fig 7 for a small value of $\omega = 2.0$ (left panel) and a large value $\omega = 90$ (right panel). In both cases, the value of h is chosen such that η lies on the first root of $J_0(\eta)$. The onset of chaos for small drive frequency indicates thermal behaviour for typical initial conditions, with small islands of regularity for others. This is consistent with similar results for small frequencies reported in [54, 59]. However, at high frequency, the regular islands distinctly dominate over the chaos. The trajectories indicate that the conservation of $\langle S^x \rangle \approx \sqrt{1-4q^2} \cos p$ [56] at high ω persists in the thermodynamic limit. That this is a signature of the underlying quantum dynamics can be readily seen in the quantum phase space representation of the Floquet Eigenstates for a large but finite N . These are shown in the corresponding lower panels of fig 7. Here, we have plotted the Spectral Average of the Husimi Q-functions of the acquired Floquet States in the TSS. Specifically, for a coherent state $|q, p\rangle$, the corresponding Spectral-Averaged Husimi distribution [60] is obtained by

$$H(q, p) \equiv \frac{1}{(2N+1)\pi} \sum_n \langle q, p | \phi^n \rangle \langle \phi^n | q, p \rangle. \quad (30)$$

The quantum phase space retains signatures of the classical phase space dynamics when $N = 100$, indicating the onset of the persistence of S^x conservation that arises from the resonance condition at high frequencies.

IV. PHASE CROSSOVER FROM THERMAL TO DMBL

The analysis of the periodically driven LMG model reveals two distinct scenarios at low and high external drive frequencies. In the former case, thermalization in accordance with FETH is seen, whereas in the latter case, DMBL is induced. As a result, we hypothesize that a macroscopic change in phase occurs due to the influence of frequency.

To demonstrate this, we investigate the IPR of the Floquet mode with smallest quasienergy for numerous frequencies and system sizes, along with the associated drive amplitude h keeping the system at a localization point. The results are shown in fig 8. In the low-frequency range $\omega \in [1.0, 9.0]$, the IPR exhibits values

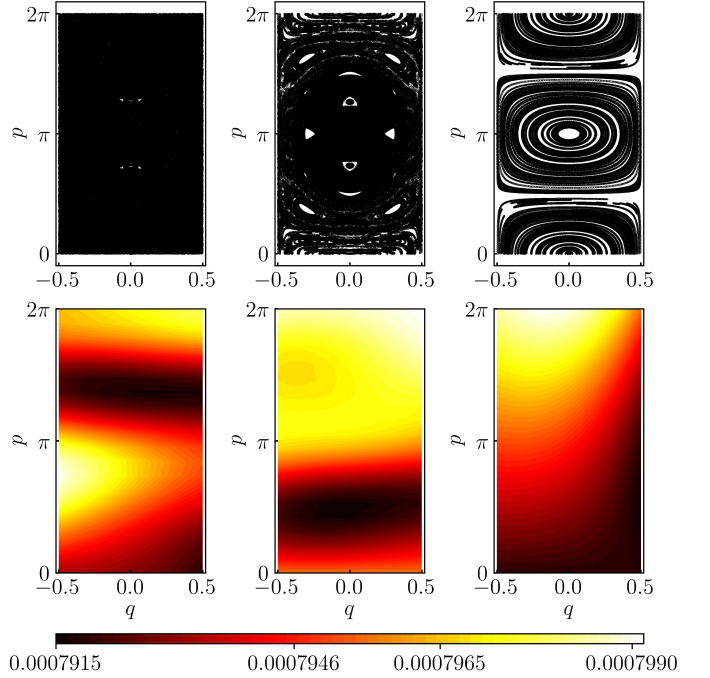


FIG. 7. Phase-space distributions at $\omega = 1.0$ (left panels), $\omega = 2.5$ (middle panels) and $\omega = 90.0$ (right panels) for 100 initial conditions. The drive amplitude h is always adjusted such that $\eta = 4h/\omega$ lies on the smallest root of $J_0(\eta)$, i.e. $\eta = 2.4048\dots$. At small $\omega = 1.0$, the classical PSOS, obtained from simulating the dynamics in eqns 29 (top left panel), shows chaotic behaviour, and at $\omega = 2.5$, regular regions start to appear. At higher $\omega = 90.0$, the dominance of regular dynamics can be readily seen (top right panel). The bottom panels plot the corresponding Spectral-Averaged Husimi-Q function, obtained from the Floquet modes $|\phi^n\rangle$ using eqn. 30, and setting $N = 100$. The $\omega = 1.0$ case (bottom left panel) has a dispersed distribution in colour. This is consistent with the chaotic behaviour seen in the continuum limit. At $\omega = 2.5$ (bottom middle panel), there is a partial regular pattern observed together with a dispersed pattern. In the $\omega = 90$ -case (bottom right panel), the distribution has distinct colour contrasts, which is consistent with the regular dynamics pattern seen in the continuum limit.

well below unity. Moreover, the IPR gradually diminishes with increasing system size, following a system size inverse proportional trend. Moreover, as can be seen in the bottom panel of the same figure, when the dynamics is simulated for smaller ωs , the fall of $\phi_{IPR}(N)$ asymptotically approaches one that characterizes a fully thermal state, where $\phi_{IPR}(N) \sim 1/N$ in the TSS. This confirms the participation distribution (as shown in the bottom panel). As in the limit $N \rightarrow \infty$, the inverse participation ratio (IPR) tends towards zero, indicating a fully delocalized state. Contrast this with the IPR plots shown in the bottom left panel of fig 2 for the integrable TFIM. The plots reveal The top panel of fig. 8 also reveals a gradual increase in the unity towards unity of IPR over a certain frequency range, specifically at $\omega \approx 5$. In addition, the rise does not cross with those for different values

480 of N , suggesting the onset of a phase crossover [42, 61].
 481 As the size of the system increases, the crossover region
 482 becomes smoother, rather than sharper.

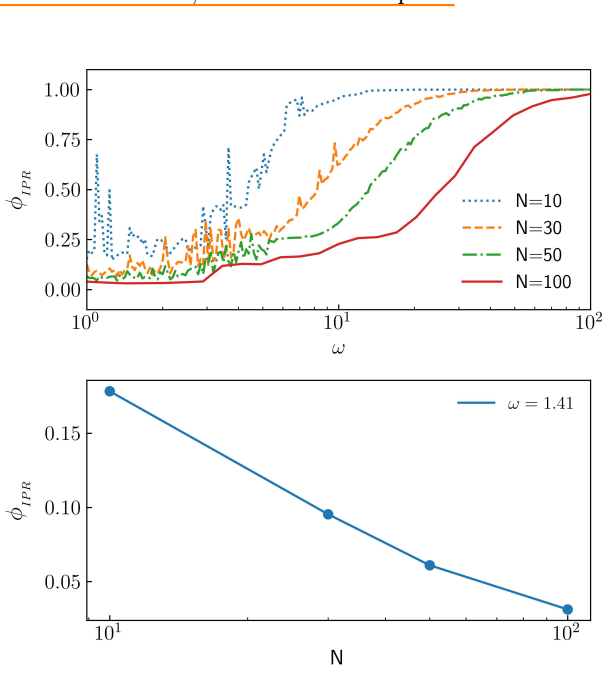


FIG. 8. IPR is plotted (top panel, ordinate) for a range of $\omega \in [1, 100]$ (top panel, abscissa) for four different $N = 10, 30, 50, 100$ at root of $J_0(\eta)$. At small ω upto $\omega \sim 10$ IPR founds to be very small and rises slowly upto unity (fully localized) at higher frequencies. At bottom panel IPR (ordinate) is plotted for different $N = 10, 30, 50, 100$ (bottom panel, abscissa) for a random small $\omega \sim 1$ at root of $J_0(\eta)$ from the values from top panel. IPR falls as inversely proportional to N , indicating an approach to a fully distributed (thermal) state. The smooth rise in IPR defines a phase crossover (top panel) between a fully thermal phase to a fully localized phase.

483

We can also look at this crossover more clearly in the plots of the heating rate of the system, defined simply by the expectation value of the Hamiltonian, $\langle \hat{H}(t) \rangle$. We have carried out the numerical evaluation from the simulated dynamics over $t = 500T$. When the system is adequately described by FETH, the temporal fluctuations in the Hamiltonian, defined by $\langle H \rangle_{std}^2 \equiv \overline{\langle \hat{H} \rangle^2} - \overline{\langle \hat{H} \rangle}^2$ (see eqn 3), are minimal in the thermodynamic limit, as the spread of states leads to a limited standard deviation [62]. Conversely, the onset of athermal behavior is indicated by nonzero fluctuations in time. If we set the initial state to the fully polarized state in the TSS (given by $|s_N\rangle$), then the onset of freezing, together with DMBL, will result in nearly infinite hysteresis in the ensuing dynamics, causing $|\psi\rangle(t) \approx |s_N\rangle \forall t$. From eqn. 18, we can clearly see that this will lead to a linearly rising dependence on ω in $\langle H \rangle_{std}$ as long as we stick to a localization point given by a fixed h/ω [63]. All these observations are corroborated by the heating rate plots in figure 9.

484

485

486

487

488

489

490

491

492

493

494

495

496

497

498

499

500

501

502

503

504

505

506

507

508

509

510

511

512

513

514

515

516

517

518

519

520

521

522

523

524

525

526

527

528

529

530

531

532

533

534

535

536

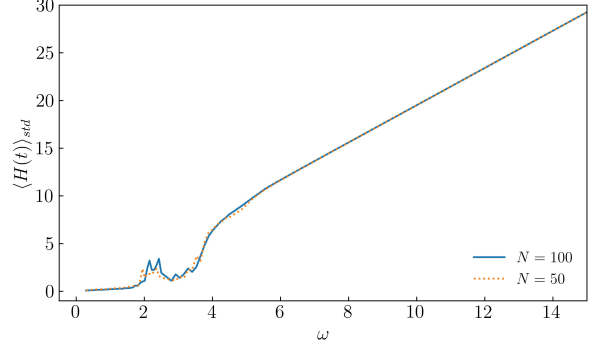


FIG. 9. The standard deviation of the heating rate, denoted by $\langle H \rangle_{std}$, calculated over a span of $t = 500T$ for two system sizes. Here, h is varied to keep $\eta = 4h/\omega$ at the first root of $J_0(\eta)$. A nonsingular rise has been identified at $\omega \approx 4.0$. $\langle H \rangle_{std}$ exhibits a diminutive magnitude below that value of ω , while a linear rise is observed at higher frequencies, consistent with freezing. A vanishingly small standard deviation for $\omega \ll 4.0$ indicates the presence of a thermal region, whereas a larger finite standard deviation suggests the existence of athermal behavior. The small peaks observed at $\omega \in [2, 4]$ are finite-size effects that disappear in the thermodynamic limit.

506 V. CONCLUSION AND OUTLOOK

507 We have delved into the onset of freezing and phase
 508 cross-over in 1D spin systems driven by a time-periodic
 509 transverse field, contrasting the responses in the Trans-
 510 verse Field Ising Model (TFIM) with that of the
 511 long-range Lipkin-Meshkov-Glick Model (LMG). The
 512 parametrization of DMBL is based on the Inverse Par-
 513 ticipation Ratio (IPR) of the Floquet eigenstates. Our
 514 investigations compared the IPRs from both models nu-
 515 merically, and found the emergence of thermal behavior
 516 at low frequencies and freezing at high frequencies for
 517 the LMG model, the latter a direct consequence of the
 518 appearance of additional approximately conserved quan-
 519 tities.

520 Long-range spins exhibit strong localization in spin-
 521 coordinate space for the LMG model when the drive fre-
 522 quency is $\omega \gg J$, where J represents the spin exchange
 523 energy. The localization of the LMG model occurs at
 524 specific resonance points of the drive frequency ω and
 525 amplitude h , at $J_0(4h/\omega) = 0$, $\omega \gg J$. This is ap-
 526 parently similar to the phenomenon of Dynamical Freez-
 527 ing (DMF) in the Transverse Field Ising Model (TFIM),
 528 where comparable localization at resonance points, de-
 529 termined by the roots of $J_0(2h/\omega)$, occurs due to the
 530 onset of an additional approximate conservation in the
 531 transverse field itself. However, a key difference is the
 532 thermal behaviour of the LMG model at low frequen-
 533 cies. Plots of the IPR for a range of frequencies along
 534 the resonance manifold exhibits a smooth increase in IPR
 535 yielding a quantum phase-crossover from a thermal phase
 536 governed by the Floquet Eigenstate Thermalization Hy-

pothesis (FETH) to a Dynamically Many-Body localized phase (DMBL). This crossover is absent in the TFIM, as can be readily seen in the significant magnitude of the inverse participation ratio (IPR) even at low frequencies. Thus, the suppression of thermalization through

Dynamical Many Body Localization in long-range systems can be controlled via Floquet engineering, even in clean systems without any disorder. Thus, periodically driven long-range spin systems are an excellent tool for investigating disorder-free Many Body Localization, as

can be readily seen via the IPR of its Floquet modes. There are several unexplored indicators of DMBL, such as entanglement entropy and level statistics [10], which we defer to future studies. In addition, Halpern in 2019 proposed a quantum engine based on MBL[11] which works between strong localized and thermal phases of

the system. In our proposed LMG model, tuning the system parameters by bringing them to the resonance points, then adiabatically cycling the frequency from the thermal region to the DMBL region, can achieve a similar engine without going through a phase transition.

A. Acknowledgements:

- One of the authors, MR acknowledges The University of Burdwan for support via a state-funded fellowship. AR acknowledges support from the University Grants Commission (UGC) of India, via BSR Startup Grant No. F.30-425/2018(BSR), as well as from the Science and Engineering Research Board (SERB) Core Research Grant No. CRG/2018/004002.
-
- [1] S. Bordia Pranjal, Lüschen Henrik, Nature Physics **13**, 460 (2017).
- [2] S. Sahoo, I. Schneider, and S. Eggert, (2019), arXiv:1906.00004 [cond-mat.str-el].
- [3] A. Das, Phys. Rev. B **82**, 172402 (2010).
- [4] G. B. Mbeng, A. Russomanno, and G. E. Santoro, (2020), arXiv:2009.09208 [quant-ph].
- [5] H. S. Yamada and K. S. Ikeda, Phys. Rev. E **105**, 054201 (2022).
- [6] A. Roy and A. Das, Phys. Rev. B **91**, 121106 (2015).
- [7] H. Li, B. Shapiro, and T. Kottos, Phys. Rev. B **98**, 121101 (2018).
- [8] A. Eckardt and E. Anisimovas, New Journal of Physics **17**, 093039 (2015).
- [9] L. Zhang, V. Khemani, and D. A. Huse, Phys. Rev. B **94**, 224202 (2016).
- [10] V. Khemani, A. Lazarides, R. Moessner, and S. L. Sondhi, Phys. Rev. Lett. **116**, 250401 (2016).
- [11] N. Yunger Halpern, C. D. White, S. Gopalakrishnan, and G. Refael, Phys. Rev. B **99**, 024203 (2019).
- [12] T. Nag, S. Roy, A. Dutta, and D. Sen, Phys. Rev. B **89**, 165425 (2014).
- [13] G. Carleo, F. Becca, M. Schiró, and M. Fabrizio, Scientific Reports **2**, 243 (2012).
- [14] S. Aditya and D. Sen, (2023), arXiv:2305.06056 [cond-mat.stat-mech].
- [15] M. Schiulaz, A. Silva, and M. Müller, Phys. Rev. B **91**, 184202 (2015).
- [16] T. Grover and M. P. A. Fisher, **2014**, P10010.
- [17] Z. Papić, E. M. Stoudenmire, and D. A. Abanin, Annals of Physics **362**, 714 (2015).
- [18] A. Smith, J. Knolle, D. L. Kovrzhin, and R. Moessner, Phys. Rev. Lett. **118**, 266601 (2017).
- [19] O. Hart, S. Gopalakrishnan, and C. Castelnovo, Phys. Rev. Lett. **126**, 227202 (2021).
- [20] H. Lipkin, N. Meshkov, and A. Glick, Nuclear Physics **62**, 188 (1965).
- [21] N. Meshkov, A. Glick, and H. Lipkin, Nuclear Physics **62**, 199 (1965).
- [22] A. Glick, H. Lipkin, and N. Meshkov, Nuclear Physics **62**, 211 (1965).
- [23] P. Ribeiro, J. Vidal, and R. Mosseri, Phys. Rev. E **78**, 021106 (2008).
- [24] N. Debergh and F. Stancu, Journal of Physics A: Mathematical and General **34**, 3265 (2001).
- [25] P. Titum and M. F. Maghrebi, Phys. Rev. Lett. **125**, 040602 (2020).
- [26] A. Campa, T. Dauxois, and S. Ruffo, Physics Reports **480**, 57 (2009).
- [27] E. R. S. Eisele, Theodor, Journal of Statistical Physics , 161 (1988).
- [28] A. Canning, Physica A: Statistical Mechanics and its Applications **185**, 254 (1992).
- [29] D. Vu, K. Huang, X. Li, and S. Das Sarma, Phys. Rev. Lett. **128**, 146601 (2022).
- [30] G. Misguich, V. Pasquier, and J.-M. Luck, Phys. Rev. B **94**, 155110 (2016).
- [31] M. Calixto and E. Romera, Journal of Statistical Mechanics: Theory and Experiment **2015**, P06029 (2015).
- [32] K. Fujii, Journal of Modern Physics **8**, 2042 (2017).
- [33] B. Sutherland, *Beautiful Models* (WORLD SCIENTIFIC) Chap. 2.
- [34] D. A. Abanin, E. Altman, I. Bloch, and M. Serbyn, Rev. Mod. Phys. **91**, 021001 (2019).
- [35] M. Srednicki, Phys. Rev. E **50**, 888 (1994).
- [36] M. Srednicki, Journal of Physics A: Mathematical and General **32**, 1163 (1999).
- [37] M. Holthaus, Journal of Physics B: Atomic, Molecular and Optical Physics **49**, 013001 (2015).
- [38] M. Vogl, M. Rodriguez-Vega, and G. A. Fiete, Phys. Rev. B **101**, 024303 (2020).
- [39] M. Bukov, L. D'Alessio, and A. Polkovnikov, Advances in Physics **64**, 139 (2015).
- [40] L. D'Alessio and M. Rigol, Phys. Rev. X **4**, 041048 (2014).
- [41] R. Yousefjani, S. Bose, and A. Bayat, Phys. Rev. Res. **5**, 013094 (2023).
- [42] P. Sierant, M. Lewenstein, A. Scardicchio, and J. Zakrzewski, Phys. Rev. B **107**, 115132 (2023).
- [43] R. Yousefjani, S. Bose, and A. Bayat, Phys. Rev. Res. **5**, 013094 (2023).
- [44] F. Alet and N. Laflorencie, Comptes Rendus Physique **19**, 498 (2018).

- DRAFT**
- 649 [45] S. J. Garratt and S. Roy, Phys. Rev. B **106**, 054309
 650 (2022).
 651 [46] R. B. Stinchcombe, Journal of Physics C: Solid State
 652 Physics **6**, 2459 (1973).
 653 [47] F. E. H. George Arfken, Hans Weber, *Mathematical
 654 Methods for Physicists*, 7th ed. (Academic Press).
 655 [48] S. Mukherjee, A. Spracklen, D. Choudhury, N. Goldman,
 656 P. Öhberg, E. Andersson, and R. R. Thomson, New Jour-
 657 nal of Physics **17**, 115002 (2015).
 658 [49] S.-H. Lin, B. Sbierski, F. Dorfner, C. Karrasch, and
 659 F. Heidrich-Meisner, SciPost Phys. **4**, 002 (2018).
 660 [50] N. C. Murphy, R. Wortis, and W. A. Atkinson, Phys.
 661 Rev. B **83**, 184206 (2011).
 662 [51] E. J. Torres-Herrera, I. Vallejo-Fabila, A. J. Martínez-
 663 Mendoza, and L. F. Santos, Phys. Rev. E **102**, 062126
 664 (2020).
 665 [52] N. Trivedi and D. Heidarian, Progress of Theoretical
 666 Physics Supplement **160**, 296 (2005).
 667 [53] G. Misguich, V. Pasquier, and J.-M. Luck, Phys. Rev. B
 668 **94**, 155110 (2016).
 669 [54] A. Russomanno, R. Fazio, and G. E. Santoro, Euro-
 670 physics Letters **110**, 37005 (2015).
 671 [55] N. Defenu, T. Enss, M. Kastner, and G. Morigi, Phys.
 672 Rev. Lett. **121**, 240403 (2018).
 673 [56] T. Mori, Journal of Physics A: Mathematical and The-
 674 retical **52**, 054001 (2019).
 675 [57] J. Johansson, P. Nation, and F. Nori, Computer Physics
 676 Communications **184**, 1234.
 677 [58] B. Sciolla and G. Biroli, Phys. Rev. Lett. **105**, 220401
 678 (2010).
 679 [59] R. A. Kidd, M. K. Olsen, and J. F. Corney, Phys. Rev.
 680 A **100**, 013625 (2019).
 681 [60] A. Bäcker, S. Fürstberger, and R. Schubert, Phys. Rev.
 682 E **70**, 036204 (2004).
 683 [61] S. Sachdev, *Quantum Phase Transitions*, 2nd ed. (Cam-
 684 bridge University Press, Cambridge, 2011).
 685 [62] P. Reimann, Journal of Statistical Mechanics: Theory
 686 and Experiment **2021**, 103106 (2021).
 687 [63] When frozen, $|\psi(t)\rangle \approx |s_N\rangle$. From eqn 18, $\langle \hat{H}_{0,1} \rangle$ are
 688 both approximately constant. Averaging the square of
 689 $\langle \hat{H}(t) \rangle$ over long times $\tau \gg T$ yields a result that goes as
 690 $h^2 + \delta$, where $\delta \sim h_0 \ll 1$. Thus, the standard deviation
 691 in time will go as $\sim h \sim \omega$, since $\eta = 4h/\omega$ is kept fixed.